EXHIBIT B

Proc. Natl. Acad. Sci. USA
Vol. 90, pp. 2486–2490, March 1993
Biochemistry

Stearoyl-acyl carrier protein Δ^9 desaturase from *Ricinus communis* is a diiron-oxo protein

(fatty acid desaturation/binuclear iron cluster/Mössbauer spectroscopy/iron-binding motif)

BRIAN G. FOX*†, JOHN SHANKLIN†‡§, CHRIS SOMERVILLE‡, AND ECKARD MÜNCK*

*Department of Chemistry, Carnegie Mellon University, Pittsburgh, PA 15213; and ‡Department of Energy Plant Research Laboratory, Michigan State University, East Lansing, MI 48824

Communicated by Helmut Beinert, November 30, 1992

ABSTRACT **A gene encoding stearoyl-acyl carrier protein Δ^9 desaturase (EC 1.14.99.6) from castor was expressed in *Escherichia coli*. The purified catalytically active enzyme contained four atoms of iron per homodimer. The desaturase was studied in two oxidation states with Mössbauer spectroscopy in applied fields up to 6.0 T. These studies show conclusively that the oxidized enzyme contains two (identical) clusters consisting of a pair of antiferromagnetically coupled ($J > 60$ cm^{-1}, $H = JS_1 \cdot S_2$) Fe^{3+} sites. The diferric cluster exhibited absorption bands from 300 to 355 nm; addition of azide elicited a charge transfer band at 450 nm. In the presence of dithionite, the clusters were reduced to the diferrous state. Addition of stearoyl-CoA and O_2 returned the clusters to the diferric state. These properties are consistent with assigning the desaturase to the class of O_2-activating proteins containing diiron-oxo clusters, most notably ribonucleotide reductase and methane monooxygenase hydroxylase. Comparison of the primary structures for these three catalytically diverse proteins revealed a conserved pair of the amino acid sequence -(Asp/Glu)-Glu-Xaa-Arg-His- separated by ≈100 amino acids. Since each of these proteins can catalyze O_2-dependent cleavage of unactivated C—H bonds, we propose that these amino acid sequences represent a biological motif used for the creation of reactive catalytic intermediates. Thus, eukaryotic fatty acid desaturation may proceed via enzymatic generation of a high-valent iron-oxo species derived from the diiron cluster.**

Fatty acids are synthesized in the plastid of higher plants by the acyl carrier protein (ACP) pathway (1). The penultimate product, stearoyl-ACP, is desaturated to oleoyl-ACP by the soluble enzyme stearoyl-ACP Δ^9 desaturase (EC 1.14.99.6) in the presence of O_2, NAD(P)H, NAD(P)H ferredoxin oxidoreductase, and ferredoxin (2). All other known desaturases are integral membrane proteins which act upon membrane lipids. The soluble desaturase has been purified from several plant species (3–5) and shown to be a homodimer of ≈70 kDa (5). Comparison of the amino acid sequences deduced from cDNA clones (3, 4) revealed that the stearoyl Δ^9 desaturase from distantly related plant species is a highly conserved polypeptide. In contrast, no substantial homology was observed with the corresponding enzymes from animals (6).

Previous studies have shown that the desaturase (7) contains iron and is inhibited by iron chelators and cyanide, but not by carbon monoxide (2, 7). In addition, both forms of stearoyl Δ^9 desaturase (5, 7) exhibit absorbance features between 300 and 400 nm and no Soret absorption. However, detailed analysis of the metal content and the optical features have not yet been reported. Here we detail the engineering of the castor (*Ricinus communis*) desaturase into a bacterial expression system which provides large quantities of functional enzyme. Protein and metal content determinations demonstrate that the desaturase contains four atoms of catalytically essential iron. Through the use of optical and Mössbauer (see ref. 8 for a general introduction) spectroscopies, this iron is shown to reside in a diiron-oxo cluster with properties similar to clusters of hemerythrin, ribonucleotide reductase, rubrerythrin, purple acid phosphatase, and the methane monooxygenase (MMO) hydroxylase (see ref. 9 for a review).

The MMO hydroxylase (10), ribonucleotide reductase (11), and the yeast stearoyl-CoA Δ^9 desaturase (12) catalyze oxygenase reactions, albeit with distinctly different chemical outcomes. For these three oxygenases, high-valent iron-oxo structures have been proposed as catalytic intermediates. A comparison of the primary structures of the castor desaturase (3), MMO hydroxylase (13), and ribonucleotide reductase (14) presented here has revealed the presence of a highly conserved set of carboxylate and histidine ligands which may constitute the iron-containing active site. Consequently, oxidative desaturation may also involve generation of a high-valent iron-oxo species derived from the diiron-oxo cluster.

MATERIALS AND METHODS

Plasmid Construction. An open reading frame corresponding to the mature castor desaturase was identified by comparison of the deduced amino acid sequences of the castor and safflower desaturases. A region of the castor cDNA (GenBank accession no. M59857) was amplified by PCR using oligonucleotides 5′-TTAACCATGGCCTCTACCCTCAAG and 3′-CGATCCATGGATCGTTTGCTTATTA. *Nco* I restriction sites were introduced at the 5′ (corresponding to Met-32) and 3′ (base pair 1565) ends of the amplified region, such that the resulting sequence could be digested and inserted into the *Nco* I site of the expression vector pET3d. The resulting plasmid (pRCMD9) was used to transform the *Escherichia coli* strain BL21(DE3).

Growth and Expression. The medium used for bacterial growth contained (per liter): Bacto tryptone, 10 g; NaCl, 5 g; and ampicillin, 50 mg. For Mössbauer studies, ^{57}Fe metal was dissolved in a minimal volume of 1 M HCl and added to provide ≈80% isotopic enrichment. Cells were grown to $OD_{600} = 0.5$ at 37°C. Expression was induced by addition of isopropyl β-D-thiogalactopyranoside (0.4 mM). Four hours after induction, cells were collected by centrifugation, washed in 40 mM Tris·HCl, pH 8.0, and stored at −70°C.

Purification. Cell paste (≈20 g) suspended in 50 ml of 40 mM Tris·HCl, pH 8.0, buffer was disrupted by a French pressure cell. The disrupted cell suspension was diluted 4-fold with buffer and DNase I (5 mg) was added. This

The publication costs of this article were defrayed in part by page charge payment. This article must therefore be hereby marked "*advertisement*" in accordance with 18 U.S.C. §1734 solely to indicate this fact.

Abbreviations: ACP, acyl carrier protein; MMO, methane monooxygenase.

†To whom reprint requests should be addressed.
§Present address: Department of Biology, Brookhaven National Laboratory, Upton, NY 11973.

mixture was centrifuged at 37,000 × *g* for 45 min at 4°C. The supernatant was diluted 2-fold with buffer and applied to a DEAE-Sephacel column (50 × 150 mm; Pharmacia) at a rate of 30 cm/hr. After loading, the column was washed with 1 liter of buffer. A 1-liter gradient of 0.0–0.3 M NaCl in 40 mM Tris·HCl, pH 8.0, buffer was applied at a rate of 15 cm/hr. The desaturase was eluted at ≈0.1 M NaCl. Fractions containing the desaturase were identified by SDS/PAGE and concentrated by ultrafiltration. The concentrated protein was applied to a Sephadex G-75 column (25 × 1000 mm) equilibrated with 50 mM Hepes, pH 7.8, containing 50 mM NaCl and 5% (vol/vol) glycerol and eluted at a rate of 5 cm/hr. Desaturase fractions were identified and concentrated as before and stored at −70°C.

Activity Assay. Activity was measured as the ferredoxin-dependent release of ^3H_2O as described in ref. 3, except that [9,10-^{3}H]stearoyl-ACP was used in place of [9,10-^{3}H]-stearoyl-CoA.

Amino Acid and Metal Content. Extinction coefficients were determined by combined optical spectroscopy and amino acid analysis of purified desaturase protein (ε_{278} = 80,410 $M^{-1}\cdot cm^{-1}$ and ε_{340} = 8400 $M^{-1}\cdot cm^{-1}$). Samples of known protein concentration were also subjected to metal analysis by atomic absorption spectroscopy. For correlation of iron content with catalytic activity, a desaturase sample was treated with *o*-bathophenanthroline disulfonate (5 mM). At appropriate time intervals (0.25–16 hr), iron removed from the desaturase was determined optically at 520 nm. The chelator-treated desaturase was then desalted by using a Sephadex G-50 spun column. The protein concentration of the chelator-free desaturase was determined optically and the remaining desaturase activity was determined as described above.

Spectroscopic Methods. Concentrations of the desaturase were determined by optical spectroscopy. Sodium azide (4 M in 100 mM Hepes, pH 7.8) was slowly added to the desaturase to a final concentration of 0.8 M. The desaturase was reduced by the addition of dithionite solution (≈1 electron per iron) followed by equilibration for 15 min at 25°C.

RESULTS

Physical and Catalytic Properties. A recombinant castor stearoyl-ACP desaturase lacking the putative transit peptide was constructed, using Met-32 as the translation initiation site. This construct resulted in the addition of one amino acid to the mature desaturase (3). Expression of this cDNA allowed the accumulation of the desaturase to 15–30% of total soluble protein. Following a two-step purification, ≈250 mg of desaturase was obtained from 20 g of cell paste. As judged by SDS/PAGE, the desaturase was greater than 95% pure and appeared as a single band of 37 kDa. Gel filtration measurements showed the recombinant desaturase had molecular mass of 75 kDa, consistent with the α_2 quaternary structure observed for all other higher plant stearoyl-ACP Δ^9 desaturases. The catalytic activity (≈10 milliunits/mg) was comparable to that of the best previously available enzyme preparations. These characterizations demonstrate that the recombinant plant desaturase has been correctly assembled into a catalytically active homodimer fully representative of the native plant enzyme.

Amino Acid and Metal Content. The measured amino acid content closely matched that predicted from the cDNA sequence, indicating a molecular mass of 83,550 Da. Correlated amino acid and metal analysis showed that the desaturase contained 3.85 ± 0.25 mol of iron per mol of holoprotein. No other metals were detected by atomic absorption, and no flavin, inorganic sulfide, or heme was present. Previous studies have suggested the requirement for iron in the soluble desaturase reaction (2). However, both the ferredoxin reductase and the ferredoxin contain cofactors or metal ions which may potentially interact with these inhibitors. As shown in Fig. 1, the progressive removal of iron from the purified desaturase resulted in the concomitant loss of enzymatic activity. Thus, we conclude iron is essential for stearoyl-ACP Δ^9 desaturase activity. At present, reincorporation of iron into the apoprotein has not been achieved.

Spectroscopic Characterization. Absorbance features (solid line of Fig. 2) were observed at 300–355 nm and 475 nm. Addition of sodium azide gave rise to a new complex with an absorption maximum at 345 nm (broken line in Fig. 2). In addition, the weak band observed at 475 nm was replaced by a more intense band at 450 nm. The optical properties described here are essentially the same as those of the corresponding complexes of methemerythrin and ribonucleotide reductase, proteins known to contain μ-oxo-bridged diiron clusters with a primary ligation sphere of oxygen and nitrogen ligands.

Optical spectra (Fig. 3) show that ≈4 electrons per molecule of desaturase were required to complete the reductive titration. The ε_{340} = 8000 $M^{-1}\cdot cm^{-1}$ calculated from the *Inset* to Fig. 3 is within 5% of that determined by optical spectroscopy and amino acid analysis, suggesting that all iron contained in the desaturase was Fe^{3+} and was converted to Fe^{2+} during the titration. No intermediates with a distinct optical spectrum were observed during the reductive titration. Likewise, no EPR signals were observed when less than 4 electrons were added per molecule of desaturase. The absence of low-temperature EPR signals in the desaturase strongly suggests that all iron must be present in complexes of either integer- or zero-electronic spin.

Fig. 4 shows Mössbauer spectra of the ^{57}Fe-enriched desaturase recorded at 4.2 K in zero magnetic field. The spectrum of the dithionite-reduced enzyme (Fig. 4, spectrum A) consists of a doublet with (average) quadrupole splitting, $\Delta E_Q \approx 3.2$ mm/s, and isomer shift, $\delta = 1.30$ mm/s. These parameters are typical of high-spin Fe^{2+} in a 5- or 6-coordinate environment of oxygen and nitrogen ligands. The 180-K data (not shown) indicate that the spectrum consists of two doublets of equal proportion. In fact, the 4.2-K spectrum is best represented as a superposition of two doublets. Least-squares fitting parameters are listed in Table 1. Fig. 4, spectrum B, shows the Mössbauer spectrum of the desaturase as isolated under aerobic conditions. Comparison with spectrum A shows that the as-isolated enzyme contained a fraction (19%) of high-spin Fe^{2+} with the same Mössbauer parameters as the dithionite-reduced desaturase. Examination of the optical spectrum obtained from this sample revealed that the ratio A_{340}/A_{278} was lower than expected (16%) from the extinction coefficient measurements, suggesting the high-spin Fe^{2+} fraction in the as-isolated enzyme was the reduced desaturase. The remaining iron in the as-isolated enzyme was contained in two quadrupole doublets. The majority species, species 1, representing ≈66% of total iron

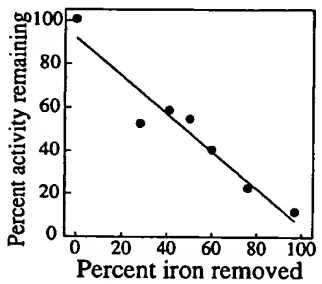

FIG. 1. Correlation between iron content and enzymatic activity. Protein data: 3.8 mol of iron per mol of protein; specific activity of 16 milliunits/mg.

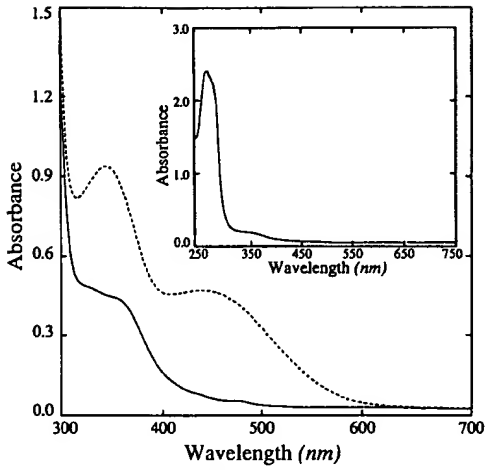

FIG. 2. Optical spectra of the oxidized desaturase (solid line) and the oxidized desaturase plus 0.8 M sodium azide (broken line). Protein data: 50 μM protein; 3.9 mol of iron per mol of protein. (*Inset*) Oxidized desaturase, expanded absorbance scale.

(or 81% of nonferrous iron), has ΔE_Q = 1.54 mm/s and δ = 0.53 mm/s, whereas the minority species, species 2, representing ≈15% of total iron, has ΔE_Q = 0.72 mm/s and δ = 0.50 mm/s. The splittings of both doublets were found to be independent of temperature in the range 4.2–180 K. The solid line drawn through the data is a least-squares fit to the contributions of the reduced enzyme and species 1 and 2; the contribution of species 2 has been outlined above the data.

Fig. 5 shows 4.2-K Mössbauer spectra of the dithionite-reduced (A) and as-isolated desaturase recorded in a 6.0-T (tesla) applied field. For clarity, the 19% contribution of the reduced enzyme has been subtracted from the raw data of the as-isolated enzyme. The resulting spectrum (B) has features typical of diamagnetic material. This is confirmed by a computer simulation (solid line drawn through spectrum B of Fig. 5) generated with the assumption that the iron atoms of both species 1 and 2 reside in environments with electronic spin S = 0.

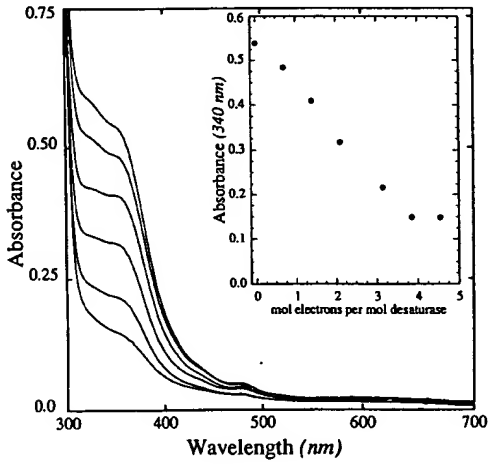

FIG. 3. Reductive titration of the desaturase. (*Inset*) Decrease in optical absorbance at 340 nm versus mol of electrons added per mol of desaturase. The absorbance of the final titration point includes contributions from both the methyl viologen radical state and sodium dithionite anion. Protein data: 79 nmol of protein in 0.85 ml of 50 mM Hepes, pH 7.8, containing 5 μM methyl viologen; 3.9 mol of iron per mol of protein.

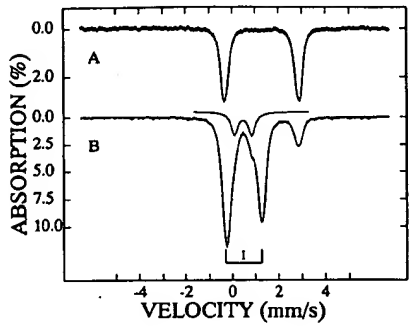

FIG. 4. Zero-field Mössbauer spectra of the dithionite-reduced (A) and as-isolated (B) desaturase recorded at 4.2 K. The solid lines are least-squares fits to the spectra using the parameters listed in Table 1. In B, the doublet of species 1 is indicated by the brackets; the doublet of species 2 is drawn separately above the data. Protein data: 250 nmol of protein in 0.25 ml of 50 mM Hepes, pH 7.8; 3.9 mol of iron per mol of protein.

The Mössbauer properties of both species 1 and 2 are compatible with either a low-spin (S = 0) Fe^{2+} configuration or antiferromagnetically spin-coupled Fe^{3+}. A low-spin Fe^{2+} assignment is chemically unreasonable, however, since reduction of the desaturase by ≈1 electron per iron produces the high-spin Fe^{2+} species of Fig. 4, spectrum A. The present observations can be reconciled if species 1 and 2 represent antiferromagnetically coupled high-spin Fe^{3+} sites.¶ Therefore, we suggest that species 1 and 2 represent the diferric cluster of the oxidized desaturase. The Mössbauer properties of the desaturase shown in Table 1 strongly resemble those of the diiron-oxo clusters found in rubrerythrin, the MMO hydroxylase, ribonucleotide reductase, hemerythrin, and purple acid phosphatase (9).

The oxo-bridge present in the diferric clusters of hemerythrin and ribonucleotide reductase provides a strong antiferromagnetic exchange pathway (exchange coupling constant $J > 200$ cm^{-1}, $H_{ex} = JS_1 \cdot S_2$, $S_1 = S_2 = 5/2$) between the two ferric sites. In contrast, the diferric cluster of the MMO hydroxylase (bridging ligands unknown, but probably not oxo) exhibits relatively weak exchange coupling ($J \approx 15$ cm^{-1}) (B.G.F. and E.M., unpublished data). As a result of the weaker coupling, the first excited spin multiplet (S = 1) of the diferric MMO hydroxylase is appreciably populated at 20 K. Consequently, Mössbauer spectra taken in strong applied fields exhibit paramagnetic structure associated with the S = 1 multiplet. This property can be used to estimate J by Mössbauer spectroscopy. For the oxidized desaturase, the 6.0-T spectrum recorded at 60 K was identical to spectrum B in Fig. 5, suggesting that $J > 60$ cm^{-1}.

The 6.0-T spectrum of the reduced desaturase (Fig. 5, spectrum A) shows that the electronic ground state of the diferrous cluster is paramagnetic, as demonstrated by the presence of sizable magnetic hyperfine interactions (for comparison, a spectrum calculated for a diamagnetic diferrous cluster is shown above the data). The observation of paramagnetic hyperfine structure rules out antiferromagnetic coupling between the ferrous sites that is larger than the

¶The values of ΔE_Q and δ, the temperature independence of ΔE_Q, and the observed diamagnetism all suggest that species 2, like species 1, represents a diferric cluster. If species 2 would represent a low-spin Fe^{2+} species, it should persist after the addition of sodium dithionite, in contrast to the experimental result of Fig. 4, spectrum A. We have recently observed pH-dependent equilibrium changes in the quadrupole patterns of the diferric cluster of the MMO hydroxylase (B.G.F. and E.M., unpublished data). Thus, the presence of species 1 and 2 could represent a pH-dependent equilibrium.

Table 1. Mössbauer properties of the desaturase

State	δ, mm/s	ΔE_Q, mm/s	T, K
Diferrous	1.24	2.75	180
	1.24	3.24	180
	1.30	3.04	4.2
	1.30	3.36	4.2
Diferric			
Species 1 (81%)	0.53	1.54	4.2
Species 2	0.50	0.74	4.2

Isomer shifts are relative to iron metal at 298 K. Values are for two inequivalent iron sites of equal proportion in the diferrous state.

zero-field splittings of the ferrous ions, suggesting that $J < 15$ cm^{-1} for the diferrous cluster.

Although the high-spin Fe^{2+} component of Fig. 4, spectrum B, has parameters similar to the diferrous cluster, this component could arise from adventitiously bound Fe^{2+}. To further define the nature of this component, stearoyl-CoA and ACP were added to an aliquot of the sample used to generate spectrum B of Fig. 4 and the mixture was incubated at 4°C for 1 hr. After this treatment, the intensity of the Fe^{2+} component had decreased from 19% to 7% without generation of mononuclear Fe^{3+}. Thus, the addition of substrate promoted catalytic oxidation of the diferrous cluster to the diferric form. Interestingly, the intensity of minority species 2 declined similarly after this treatment, with transfer of absorption into the spectral region of species 1.

Desaturase Primary Structure. Although both ribonucleotide reductase and hemerythrin contain diiron-oxo clusters, the x-ray structures clearly show no substantial homology in the primary ligation sphere (14, 15). Similarly, little sequence homology was observed between the desaturase (3) and hemerythrin (15). However, the desaturase subunit contains a pair of the amino acid sequence -(Asp/Glu)-Glu-Xaa-Arg-His- analogous to the known iron-binding sites of ribonucleotide reductase (14) and to the proposed sites of the MMO hydroxylase (13, 16) (see Fig. 6). On the basis of spectroscopic similarities between the desaturase, ribonucleotide reductase, and the MMO hydroxylase reported here, we propose that these sequences represent the iron-binding sites of the desaturase cluster. Since a pair of these sequences are present in each subunit of the desaturase, we further propose

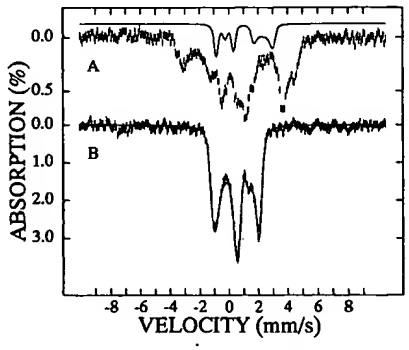

FIG. 5. High-field Mössbauer spectra of the reduced and oxidized desaturase recorded at 4.2 K in a 6.0-T applied field. The samples were the same as those of Fig. 4; the 19% contribution of spectrum A was subtracted from the raw data to provide spectrum B. The solid line above A, representing 20% of the spectral area, was computed assuming that the diferrous cluster had a diamagnetic ground state. The solid line drawn through the data of B was computed using the parameters listed in Table 1 and assuming that species 1 and 2 are diamagnetic. The following values were used for the asymmetry parameter η of the quadrupole interactions: $\eta(1) = 1$ and $\eta(2) = 0.2$. These values are uncertain but do not affect the conclusions regarding the diamagnetism of the cluster.

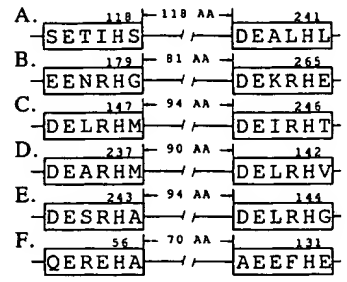

FIG. 6. Primary sequence homologies of diiron-oxo proteins capable of reaction with O_2. A, ribonucleotide reductase (14); B, stearoyl-ACP desaturase (3); C, MMO hydroxylase (13); D, phenol hydroxylase (17); E, toluene-4-monooxygenase (18); and F, rubrerythrin (19). Presently, no catalytic reaction with O_2 has been reported for rubrerythrin.

that the dimeric desaturase contains a pair of identical diiron-oxo clusters, fully accounting for the analytically and spectroscopically detected iron.

DISCUSSION

Expression of the recombinant stearoyl-ACP Δ^9 desaturase in *E. coli* has provided sufficient amounts of the desaturase to initiate detailed characterizations of the desaturase active site (20) and the reaction mechanism (21) of oxidative fatty acid desaturation. Here we provide evidence for the presence of a catalytically essential diiron-oxo cluster in the stearoyl Δ^9 desaturase.

The oxidized desaturase exhibits absorbance features between 300 and 350 nm. For methemerythrin, these features have been assigned as ligand-to-metal charge-transfer transitions arising from the Fe—O—Fe bond of a μ-oxo-bridged diiron cluster (9). A similar assignment appears to be appropriate for the desaturase. Hemerythrin also exhibits exogenous (Cl^-, HO^-, N_3^-) ligand-to-metal charge-transfer bands in the region from 400 to 500 nm. It is therefore reasonable to assign the weak absorbance band observed at 475 nm in the oxidized desaturase and the stronger band observed at 450 nm in the presence of azide (see Fig. 2) to such a transition. As O_2 binding is likely required during the catalytic cycle, the binding of azide to the desaturase cluster indicates the presence of accessible coordination sites.

The Mössbauer data show that all iron of the α_2 desaturase belongs to two clusters of the type found in diiron-oxo proteins. The oxidized clusters have ΔE_Q and δ values characteristic of high-spin Fe^{3+} in an environment of oxygen and nitrogen ligands. The absence of low-energy charge-transfer interactions characteristic of thiolate (400–600 nm) coordination further supports this assignment. Mössbauer studies in applied magnetic fields show that the two ferric sites are antiferromagnetically coupled. The strength of the coupling, $J > 60$ cm^{-1}, is consistent with, but does not prove, the presence of an oxo bridge between the two ferric ions. The isomer shifts for the diferrous cluster are at the high end of the range of values for diiron-oxo clusters, suggesting that the coordination environment is rich in oxygenous ligands such as carboxylate and water. Since the desaturase is a homodimer and also contains two diiron clusters, it is reasonable to assume that both clusters are equivalent, with each cluster having two inequivalent iron sites in the diferrous form (see Table 1). The presence of paramagnetic hyperfine interactions in a 6.0-T applied field rules out *strong* antiferromagnetic coupling between the ferrous ions but is consistent with either ferromagnetic or *weak* antiferromagnetic coupling.

Upon computer search (GenBank release 74) of primary sequences, only 40 additional occurrences of the iron-binding sequences of Fig. 6 were identified. A majority of these were found in proteins known to contain nonheme iron and to catalyze O_2-dependent reactions. Half of these occurrences are in the iron- or manganese-containing superoxide dismutase (22), for which the x-ray structure shows that Asp-156 and His-160 are iron ligands. Isopenicillin N synthase also contains a single copy of this sequence (23). Interestingly, a high-valent iron-oxo intermediate has been proposed for this enzyme (24). For the isopenicillin N synthase from *Cephalosporium acremonium*, Asp-131, Glu-132, and His-135 are contained in the iron-binding sequence, in possible correspondence with the histidine and aspartate ligation proposed from NMR studies (25).

Recently, a diiron-oxo cluster has been observed in rubrerythrin. On the basis of a similar primary sequence analysis, two iron-binding sites were previously identified in rubrerythrin (19). The Mössbauer parameters of the desaturase and rubrerythrin are nearly identical for both redox states and are consistent with the histidine and carboxylate ligation proposed in Fig. 6. We also note that two copies of -(Asp/Glu)-Glu-Xaa-Arg-His- are observed in phenol hydroxylase (17) and toluene-4-monooxygenase (18), suggesting a diiron-oxo cluster may be present in these two oxygenases as well. Finally, for all known sequences of the soluble plant desaturase (six to date), the MMO hydroxylase (13), phenol hydroxylase, and toluene monooxygenase, histidine is always preceded by arginine within the proposed iron-binding sequence, suggesting a possible contribution to oxygenase catalysis as proposed for cytochrome *c* peroxidase (26).

It has become increasingly clear that diiron-oxo clusters are common and catalytically diverse structures. Owing to the requirement to cleave unactivated C—H bonds, oxidative desaturation may involve the generation of a reactive high-valent iron-oxo intermediate of the type proposed for the MMO hydroxylase (10). Structural variations in the ligation sphere may allow partition of the reactivity of the diiron-oxo cluster between oxidative desaturation, hydroxylation, or tyrosine radical formation. The key structural features which modulate the oxidative reactivity of protein-contained diiron-oxo clusters remain to be identified.

We thank A. A. Rangarajan and I. Widders for use of the atomic absorption spectrometer with which the metal determinations were made. J.S. and B.G.F. contributed equally to this work and should therefore both be considered first and corresponding authors. This work was supported by grants from the Department of Agriculture/National Science Foundation/Department of Energy Plant Science Center Program, the National Science Foundation (Grant DCB-891631), and the Department of Energy (Grant DE-AC02-76ER0-13338) to C.S. and by a Grant from the National Institutes of Health (Grant GM-22701) to E.M., and J.S. was a Monsanto Visiting Research Associate at Michigan State University.

1. Ohlrogge, J. B., Kuhn, D. N. & Stumpf, P. K. (1979) *Proc. Natl. Acad. Sci. USA* **76**, 1194–1198.
2. Nagai, J. & Bloch, K. (1968) *J. Biol. Chem.* **243**, 4626–4633.
3. Shanklin, J. & Somerville, C. (1991) *Proc. Natl. Acad. Sci. USA* **88**, 2510–2514.
4. Thompson, G. A., Scherer, D. E., Foxall-Van Aken, S., Kenny, J. W., Young, H. L., Shintani, D. K., Kridl, J. C. & Knauf, V. C. (1991) *Proc. Natl. Acad. Sci. USA* **88**, 2578–2582.
5. McKeon, T. A. & Stumpf, P. K. (1982) *J. Biol. Chem.* **257**, 12141–12147.
6. Thiede, M. A., Ozols, J. & Strittmatter, P. (1986) *J. Biol. Chem.* **261**, 13230–13235.
7. Strittmatter, P., Spatz, L., Corcoran, D., Rogers, M. J., Setlow, B. & Redline, R. (1974) *Proc. Natl. Acad. Sci. USA* **71**, 4565–4569.
8. Münck, E. (1978) *Methods Enzymol.* **54**, 346–379.
9. Que, L., Jr. & True, A. E. (1990) in *Progress in Inorganic Chemistry: Bioinorganic Chemistry*, ed., Lippard, S. J. (Wiley, New York), Vol. 38, pp. 97–200.
10. Fox, B. G., Borneman, J. G., Wackett, L. P. & Lipscomb, J. D. (1990) *Biochemistry* **29**, 6419–6427.
11. Elgren, T. E., Lynch, J. B., Juarez-Garcia, C., Münck, E., Sjöberg, B.-M. & Que, L., Jr. (1991) *J. Biol. Chem.* **266**, 19265–19268.
12. Buist, P. H. & Marecak, D. M. (1992) *J. Am. Chem. Soc.* **114**, 5073–5080.
13. Cardy, D. L. N., Laidler, V., Salmond, G. P. C. & Murrell, J. C. (1991) *Mol. Microbiol.* **5**, 335–342.
14. Nordlund, P., Sjöberg, B.-M. & Eklund, H. (1990) *Nature (London)* **345**, 593–598.
15. Stenkamp, R. E., Sieker, L. C. & Jensen, L. H. (1984) *J. Am. Chem. Soc.* **106**, 618–622.
16. Hendrich, M. P., Fox, B. G., Andersson, K. K., Debrunner, P. G. & Lipscomb, J. D. (1992) *J. Biol. Chem.* **267**, 261–269.
17. Nordlund, I., Powlowski, J. & Shingler, V. (1990) *J. Bacteriol.* **172**, 6826–6833.
18. Yen, K.-M., Karl, M. R., Blatt, L. M., Simon, M. J., Winter, R. B., Fausset, P. R., Lu, H. S., Harcourt, A. A. & Chen, K. K. (1991) *J. Bacteriol.* **173**, 5315–5327.
19. Kurtz, D. M., Jr. & Prickril, B. C. (1991) *Biochem. Biophys. Res. Commun.* **181**, 337–341.
20. Schneider, G., Lindqvist, Y., Shanklin, J. & Somerville, C. (1992) *J. Mol. Biol.* **225**, 561–564.
21. van de Loo, F. J., Fox, B. G. & Somerville, C. (1993) in *Lipid Metabolism in Plants*, ed. Moore, T. (CRC, Boca Raton, FL), pp. 91–126.
22. Carlioz, A., Ludwig, M. L., Stallings, W. C., Fee, J. A., Steinman, H. M. & Touati, D. (1988) *J. Biol. Chem.* **263**, 1555–1562.
23. Samson, S. M., Belagaje, R., Blankenship, D. T., Chapman, J. L., Perry, D., Skatrud, P. L., Van Frank, R. M., Abraham, E. P., Baldwin, J. E., Queener, S. W. & Ingolia, T. D. (1985) *Nature (London)* **318**, 191–194.
24. Baldwin, J. E. & Abraham, E. P. (1988) *Nat. Prod. Rep.* **5**, 129–145.
25. Ming, L.-J., Que, L., Jr., Kriauciunas, A., Frolik, C. A. & Chen, V. J. (1990) *Biochemistry* **30**, 11653–11659.
26. Poulos, T. L. & Kraut, J. (1980) *J. Biol. Chem.* **255**, 8199–8205.